The QUIJOTE TGI

R. Hoyland*[a], M. Aguiar-González[a], R. Génova-Santosa[a], F. Gómez-Reñasco[a], C. López-Caraballo[a], R. Rebolo-López[a], J.A. Rubiño-Martín[a], V. Sánchez-de la Rosa[a], A. Vega-Moreno[a], T. Viera-Curbelo[a], A. Peláez-Santos[a], R. Vignaga[a], D. Tramonte[a], F. Poidevin[a], M.R. Pérez-de-Taoro[a], E. Martínez-Gonzalez[b], B. Aja[c], E. Artal[c], J. Cagigas[c], J. L. Cano-de-Diego[c], E.M. Cuerno[c], L. de-la-Fuente[c], A. Pérez[c], D. Ortiz[c], J.V. Terán[c], E. Villa[c], L. Piccirillo[d], M. Hobson[e]

[a]Instituto de Astrofísica de Canarias (IAC), C/Vía Láctea, s/n, E-38200, La Laguna, Tenerife, Spain. 00349226005200

[b]Instituto de Física de Cantabria (IFCA), CSIC-Univ. de Cantabria, Avda. los Castros, s/n, E-39005 Santander, Spain 0034942201459

[c]Departamento de Ingeniería de Comunicaciones (DICOM), Laboratorios de I+D de Telecomunicaciones, Plaza de la Ciencia s/n, E-39005 Santander, Spain 0034942201397

[d]Jodrell Bank Centre for Astrophysics, School of Physics and Astronomy, University of Manchester, Oxford Road, Manchester M13 9PL, UK 0044161275 4194

[e]Astrophysics Group, Cavendish Laboratory, University of Cambridge, Madingley Road, Cambridge CB3 0HE 0044 1223 339992

ABSTRACT

The QUIJOTE TGI instrument is currently being assembled and tested at the IAC in Spain. The TGI is a 31 pixel 26-36 GHz polarimeter array designed to be mounted at the focus of the second QUIJOTE telescope. This follows a first telescope and multi-frequency instrument that have now been observing almost 2 years. The polarimeter design is based on the QUIET polarimeter scheme but with the addition of an extra 90º phase switch which allows for quasi-instantaneous complete QUI measurements through each detector. The advantage of this is a reduction in the systematics associated with differencing two independent radiometer channels. The polarimeters are split into a cold front end and a warm back end. The back end is a highly integrated design by engineers at DICOM. It is also sufficiently modular for testing purposes. In this presentation the high quality wide band components used in the optical design (also designed in DICOM) are presented as well as the novel cryogenic modular design. Each polarimeter chain is accessible individually and can be removed from the cryostat and replaced without having to move the remaining pixels. The optical components work over the complete Ka band showing excellent performance. Results from the sub unit measurements are presented and also a description of the novel calibration technique that allows for bandpass measurement and polar alignment. Terrestrial Calibration for this instrument is very important and will be carried out at three points in the commissioning phase: in the laboratory, at the telescope site and finally a reduce set of calibrations will be carried out on the telescope before measurements of extraterrestrial sources begin. The telescope pointing model is known to be more precise than the expected calibration precision so no further significant error will be added through the telescope optics. The integrated back-end components are presented showing the overall arrangement for mounting on the cryostat. Many of the microwave circuits are in-house designs with performances that go beyond commercially available products. Individual component performance is be presented showing for each of the sub modules

Keywords: polarization, CMBr, instrumentation, spectrometer, foregrounds, B-modes, mapping

1. INTRODUCTION

The study of the anisotropy in the Cosmic Microwave Background (CMB) provides a powerful tool to obtain high-precision constraints on the basic cosmological parameters that describe our Universe. For this reason several experiments have been mapping the intensity of these anisotropies over the last decades with increasingly higher sensitivities. All these data have successfully confirmed the ΛCDM paradigm. The Planck ESA satellite [1], which is currently flying, will produce full-sky maps with unprecedented angular resolution and sensitivity.

With the completion of these observations there has been a growing interest in studying the polarization of the CMB. Despite the fact that the polar signal is more than two orders of magnitude below that of total intensity, it is now possible to study these signals thanks to the increasing sensitivity of the instrumentation. The CMB polarization pattern is normally decomposed into the E-modes (curl-free component) and the B-modes (curl component). The E-modes were first detected by the DASI experiment [2]. The amplitude of the B modes is expected to be around an order of magnitude lower and remains undetected. Its detection would however be an important milestone in cosmology, as it would confirm the presence of gravitational waves in the primordial Universe, which would have been created by inflation, an epoch of exponential expansion of the early Universe. Furthermore, the determination of the amplitude of the B-modes will give information about the energy scale at which inflation occurred.

For the previous reasons, several experiments have been designed in the last few years to observe the CMB polarization. These experiments, apart from having high sensitivity, will need to be complemented with an accurate characterization of the polarization of the Galactic foregrounds, whose amplitude is higher than the B-mode signal. The QUIJOTE (Q-U-I JOint TEnerife) CMB experiment is one of these current observational efforts. The scientific objectives of this project are two-fold: i) to detect the imprint of the primordial B-mode signal if it has an amplitude $r \geq 0.05$ [3], and ii) to characterize the polarized foregrounds at low frequencies. This experiment will probably be unique in what concerns the second of these goals, as it is the only one observing at low frequencies (<20 GHz), and therefore will provide essential information about the polarization of the synchrotron and the anomalous microwave emissions, the two main polarized foregrounds emitting at low frequencies. These measurements will be complemented, at high frequencies (>100 GHz), by measurements from the Planck mission, that will allow the characterization of the polarization in the thermal dust emission, another important foreground which is dominant at high frequency.

The QUIJOTE-CMB experiment is a scientific collaboration between the Instituto de Astrofísica de Canarias, the Instituto de Física de Cantabria, the IDOM company, and the universities of Cantabria, Manchester and Cambridge. The whole project is made up of two phases. Phase I includes the construction of a first telescope (QT1) and two instruments: the multi-frequency instrument (MFI), operating at 10-20 GHz, and the thirty-gigahertz instrument (TGI). Phase II includes the construction of a second telescope (QT2) and a third instrument, the so-called forty-gigahertz instrument (FGI). The MFI will be dedicated primarily to the characterization of the polarized foregrounds, whereas the TGI and the FGI will be focused on B-mode science. The two telescopes will be situated in the Teide Observatory (Tenerife, Spain). At the moment of writing, the QT1 has already been deployed at the observatory and has been operating with the MFI for the past 2 years. More specific details about this project, its instrumental setup, and its scientific goals, are given in the accompanying article [3]. Further details about the MFI control system are given in [4]. In this article we present the status of the TGI.

2. THE QUIJOTE TGI DESIGN

Figure 1 shows a schematic drawing of the TGI design. The receiver consists of 4 modules which are interconnected with either waveguide of coaxial cable. The latter 3 modules form the BEM and are housed in a 19" rack The first module is cooled to between 10 and 20 kelvin in a cryostat. It includes the front-end low loss components such as the feedhorn, polarizer and OMT as well as the cryogenic Low Noise Amplifiers (LNA). The second module is an RF gain stage which includes bandpass filters and amplifiers for both the Left Hand Polar (L) and Right Hand Polar (R) branches. The third module contains the broadband 180º and 90º phase switches for both branches. The fourth module is the detection module or complex correlator. The two input branches are combined into 4 outputs. They are correlated through 180º hybrids. The latter two outputs are derived from one input channel shifted by 90º to the other. The outputs are detected through square-law detectors and passed through a low pass filter and DC amplification section.

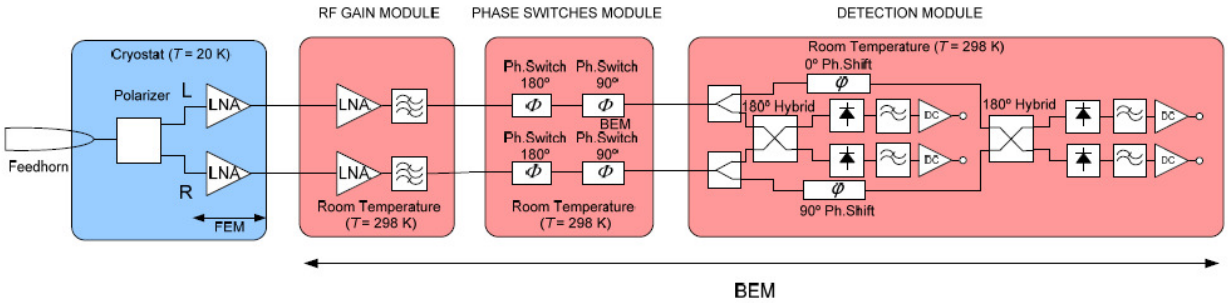

Figure 1. A schematic diagram of a TGI receiver.

Figure 2 and table 1 show the action of the phase switches on a given linearly polar signal entering the feedhorn. The phase switches modify the input by effectively adding 0º or 180º for the 180º phase switch or 0º or 90º for the 90º phase switch. It can be seen that with a 180º and 90º phase switch in both branches the relative phase between both branches can be 0º,90º,180º or 270º. The relative phase between branches gives rise to a complete set of linear polar signals at the outputs 1,2,3 and 4. If more than one output is used (this assumes the gain and bandpass are the same for each) then for a given linearly polar input, I, Q and U can be determined using the combinations in table 1.In order to reduce systematics it is desirable that each output is used individually to determine I, Q and U. A rearrangement in the table 1 shows that this can also be done using the 4 relative phase states. If all four channels are combined to give an overall value for I, Q and U then either method gives the same result. Note that there are 16 possible phase switch combinations with only 4 possible relative phases (ie there is redundancy). Using all 16 positions allows for correction of the small differences in bandpass and errors in phase between relative phase states.

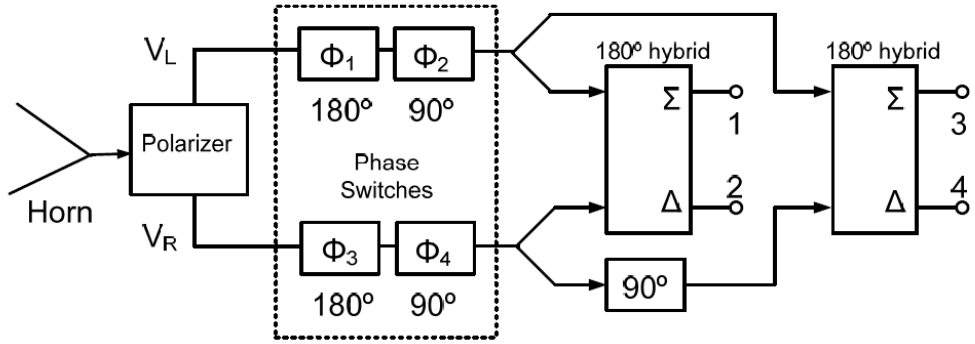

Figure 2. A schematic diagram showing the TGI signal paths in more detail.

Table 1. Table to show the effect of the phase differences between branch L and R in terms of I, Q and U of a linearly polarized signal entering the feedhorn.

Φ	I	Q	U
0º	Vd1 + Vd2 = Vd3 + Vd4	Vd1 – Vd2	Vd3 – Vd4
90º	Vd1 + Vd2 = Vd3 + Vd4	Vd3 – Vd4	Vd2 – Vd1
180º	Vd1 + Vd2 = Vd3 + Vd4	Vd2 – Vd1	Vd4 – Vd3
270º	Vd1 + Vd2 = Vd3 + Vd4	Vd4 – Vd3	Vd1 – Vd2

3. THE MECHANICAL AND CRYOGENIC IMPLEMENTATION OF THE TGI FRONTEND

3.1 The Cryostat

The front end of the TGI pixels are housed in a cryostat. Figure 3 shows two 3d views of the cryostat with the top cover removed. The left view shows how the feedhorns protrude through the cold radiation shielding. The right view shows the bulkhead with the Dual-Thompson displacer towards the top side of the cryostat and the pixel array towards the bottom side. The pixel feedthroughs are hexagonal to give the tightest packing possible. Figure 4 shows a view of the cryostat with the radiation shields removed. The feedhorn array can be clearly seen with the polarizers and OMTs. The waveguides and waveguide supports have not been included in the drawing. The cryostat includes a novel crown like thermal contact (ref:alma) which allows for ease of integration. The pixel thermal contact is a cylindrical flat surface which passes through each crown. The crown consists of tensioned aluminium fingers enclosed by a Teflon ring. The Teflon ring contracts when the cryostat is cooled pulling the crown tightly onto the pixel thermal contact. Pixels can be individually mounted and dismounted without the need to disassemble the whole cryostat.

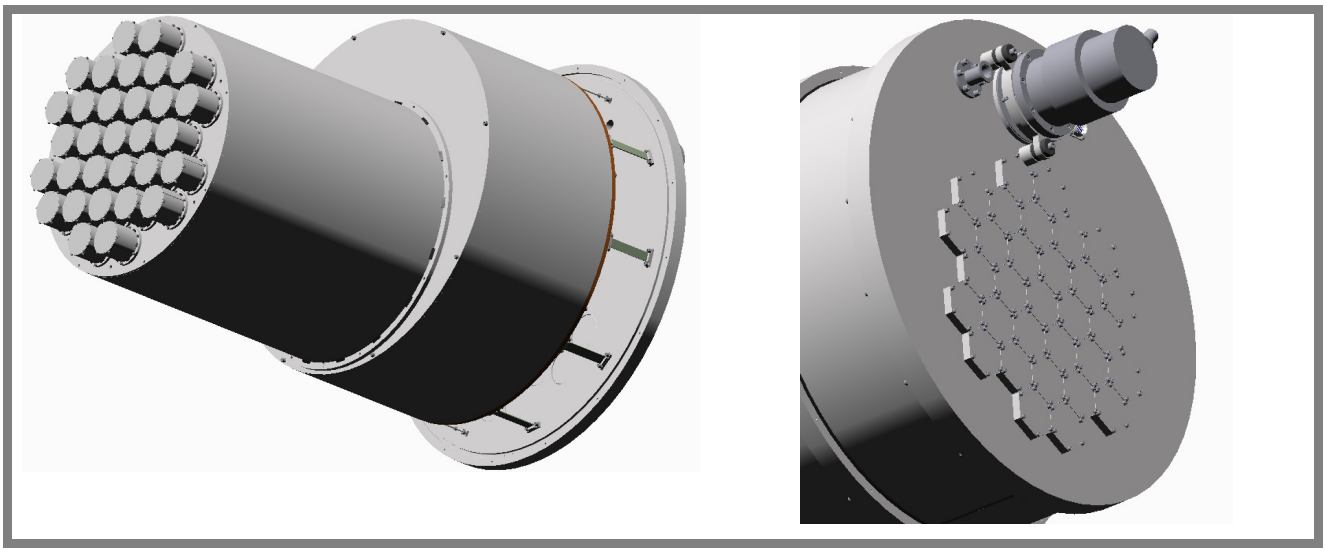

Figure 3: Two 3D views of the TGI cryostat with the top cover removed. The front shows how the 31 feedhorns protrude out of the cold radiation shielding (left) and the back (right) shows a hexagonal array which are the pixel bulkhead feedthroughs.

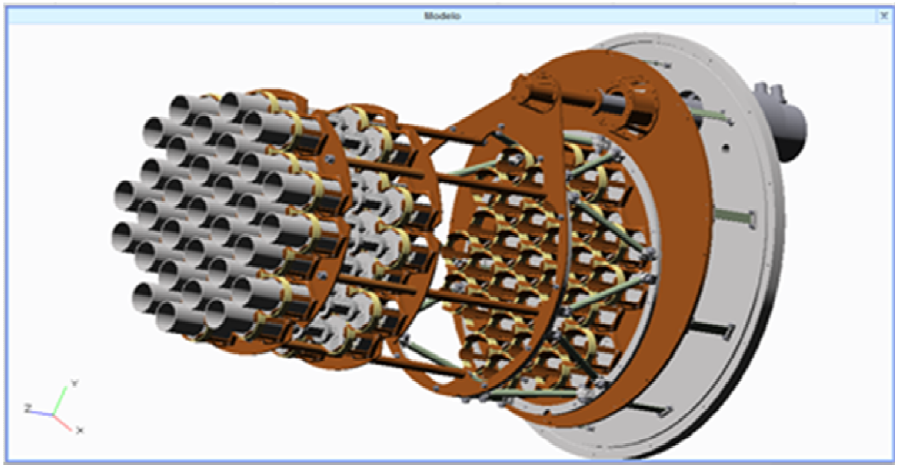

Figure 4: A 3D view of the cryostat with the radiation sheilds and top cover removed.

3.2 The Pixels

The TGI pixels are modular. The whole pixel fits within a given pixel diameter including the cryogenic harnesses needed to supply the LNAs. Figure 5 shows two views of these pixels with and without the G10 support structure. The support structure is necessary to hold the stainless steel thin-walled waveguide in place and must also have very low thermal conductivity. The G10 supports consist of 4 strips running along the pixel mounted on various circular sections. The waveguides connect the output from the LNAs to the bulkhead. A waveguide to coaxial adapter is mounted on the outside of the bulkhead. Coaxial cable connects the cryostat to the BEM rack. The cryo-harness passes through the bulkhead within the pixel diameter. An external cable connects the pixel to the LNA power supplies.

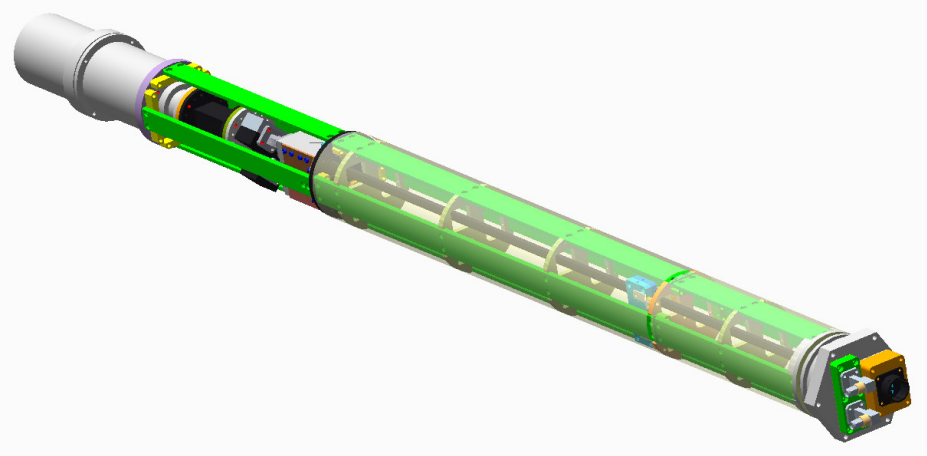

Figure 5: Two 3D views of a TGI pixel with (bottom) and without (top) the G10 support structure

4. MICROWAVE MEASUREMENTS OF SUBSYSTEMS

Each of microwave subsystems has been measured individually where possible. The measurements are presented in the following subsections.

4.1 Feedhorns

The TGI corrugated feedhorns are a novel design (ref). They have been manufactured from aluminium 6061 and are treated with alodine 1200. They are turned on a CNC lathe in 3 sections. The most critical section is the throat. This is also the most difficult to machine due to the narrow input and deep corrugations. This novel design allows the throat input to be flat and without corrugations. No degradation in performance is seen by this modification. The design maintains a > 40dB cross polarization and sidelobes < -25dB down from the main beam (see figure 7). The horn design and photo are shown in figure 6

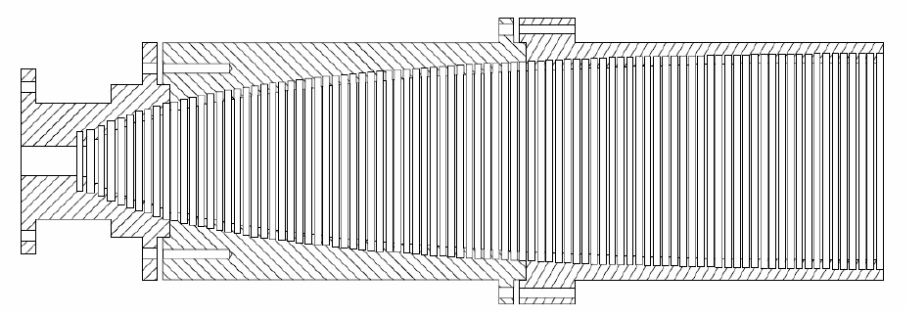

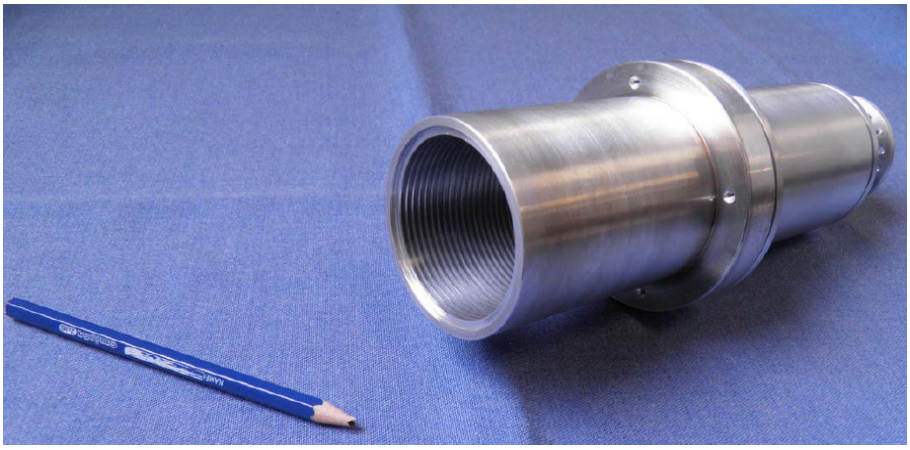

Figure 6. The 2D cross-section and photo of the TGI corrugated feedhorn

The measured S parameters and radiation pattern are shown in figure 7. It can be seen that the horn is well-matched < -20dB across the entire band and that the beam is very symmetric. The gain of the feedhorn is between 21-24dB.

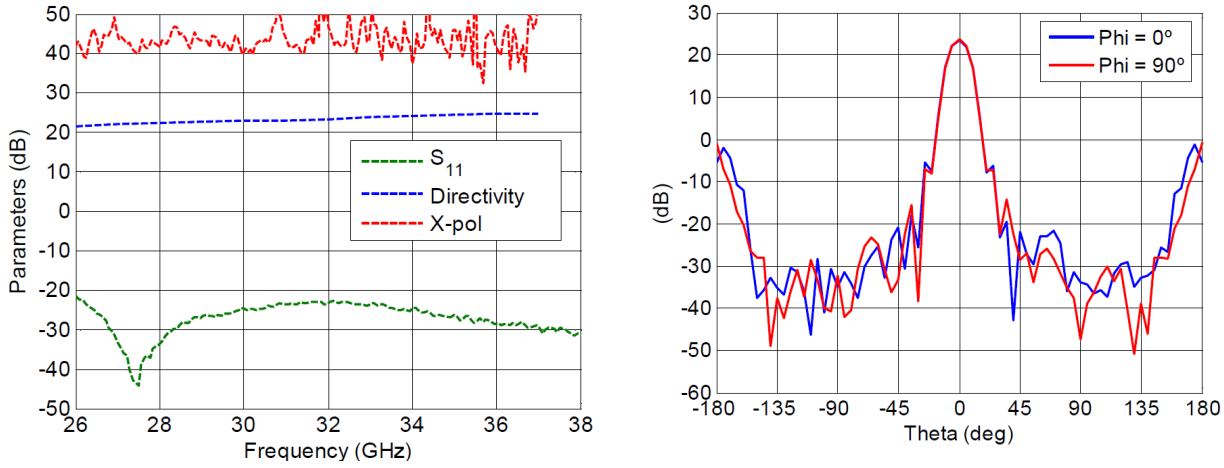

Figure 7: Graphs to show (left) main properties of the feedhorn and (right) the beam pattern

4.2 Waveguide Polarizer

The waveguide polarizer is a ridged waveguide design (ref). It can be seen from the drawing in figure 8 that the ridges are cut in the centre of each face of the square sectioned waveguide. The polarizer is electro-eroded. The ridges are different on the horizontal faces to those on the vertical faces. This gives rise to a 90º phase shift between orthogonal modes in the waveguide. Figure 8 also shows a photo of the polarizer being measured. It can be seen that square to circular adaptors are used at each end of the polarizer. The measured s-parameters are shown in figure 9. It can be seen that the return loss of both orthogonal modes is < -25dB across the entire band. The phase difference between orthogonal modes is 90º ± 1º. This is state-of-the-art performance for such a device.

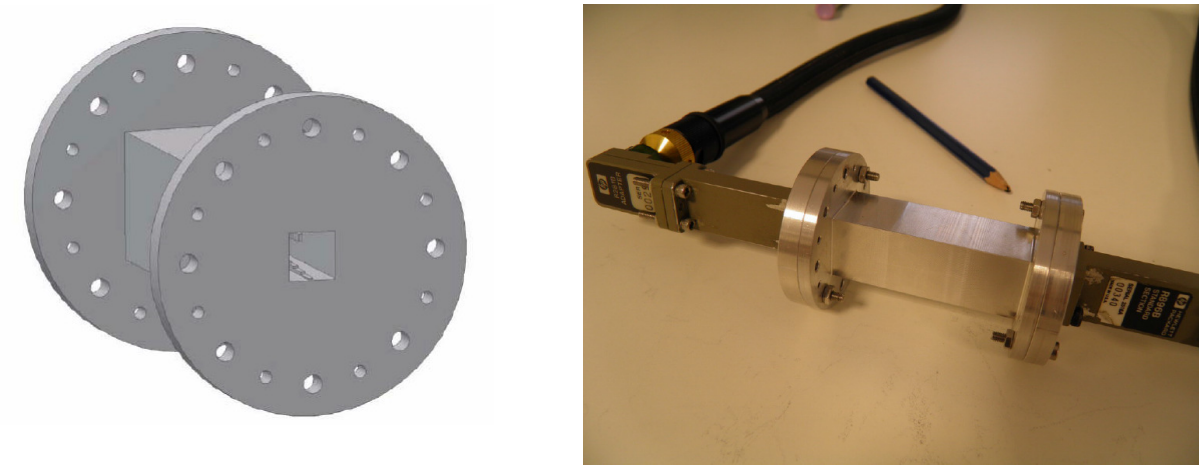

Figure 8. A 3D drawing of the polarizer (left) and a photo (right) of the polarizer being measured.

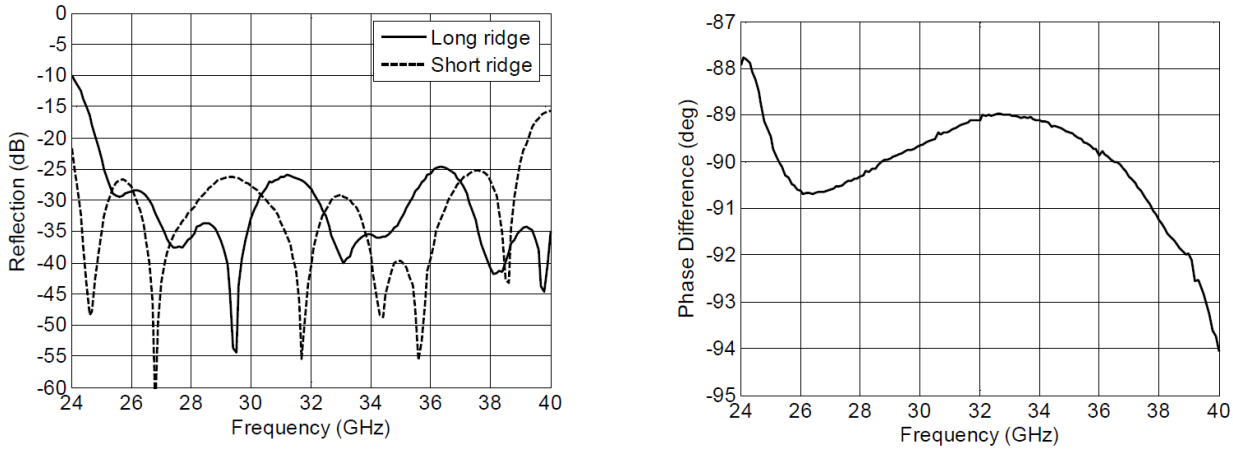

Figure 9. Graphs to show the excellent properties of the polarizer: (left) shows return loss and (right) shows the phase difference between orthogonal modes.

4.3 OMT

The TGI OMT is a modified version of the Ka band OMT presented in (ref). The difference is in the diameter of the circular waveguide at the input. This was enlarged to fit the diameter of the horn and polarizer sections. The TGI band is 26-36GHz and the Ka band 26.5-40GHz. The Ka band components are more lossy at the lower frequency limit so the circular waveguide was enlarged to avoid this loss. Figure 10 shows a photo of the finished OMT which has been CNC machined in 5 pieces. The central scattering pin can also be seen in the photo. Figure 11 shows the excellent s parameters. It can be seen that the return loss is better than -25dB across the entire band and the Isolation is better than -50 dB.

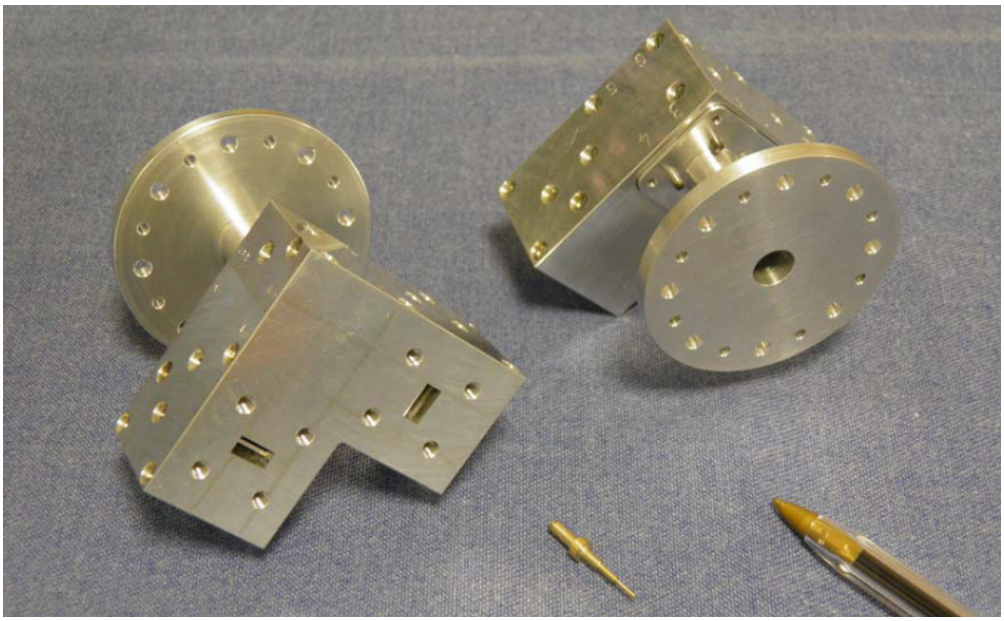

Figure 10. Photo showing the finished TGI OMT

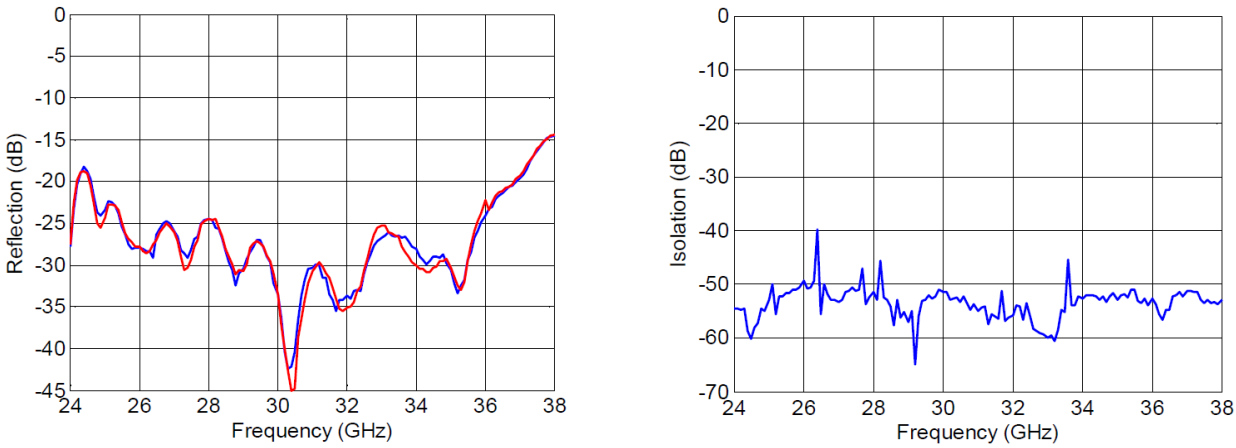

Figure 11. Graphs to show the return loss (left) and Isolation (right) of the TGI OMT

4.4 Cryogenic LNAs

The cryogenic LNA is based on a MMIC on 100 nm MHEMT technology from the Fraunhofer IAF, Freiburg, Germany, and a second MMIC low noise amplifier on 130 nm MHEMT technology from the OMMIC foundry, France (ref: B. Aja). A 5 dB attenuator has been added between both amplifiers, in order to reduce gain and to assure stability. All the DC circuitry as well as the RF circuit are included in the same box with a WR-28 waveguide input /output and a 9-pin Micro-D connector to supply the DC bias. Figure 12 shows photos of the LNA chip, microwave channel and housing. Figure 13 shows the LNA cryogenic performance. It can be seen that the LNA has about 40dB gain and a noise temperature of between 20-30K across the band when cold.

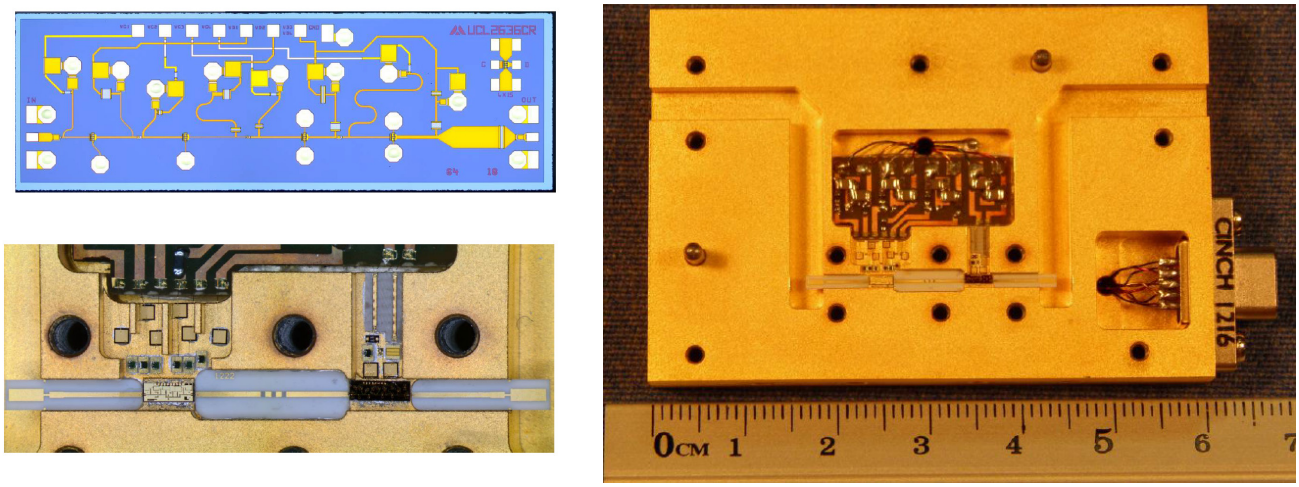

Figure 12. Photos of the cryogenic LNA: Left top: LNA MMIC, left bottom: LNA microwave channel, right: LNA housing.

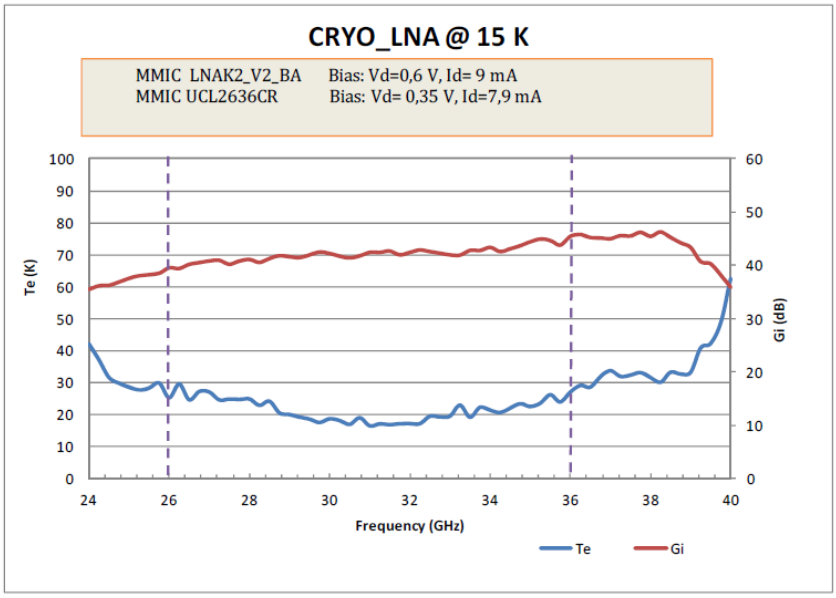

Figure 13. Graph to show the LNA noise performance at cryogenic temperature

4.5 RF Gain Module

The RF gain module is shown in figure 14. The Gain Module includes two MMIC LNAs model AMMC-6241 from Avago Technologies, and a 10 dB attenuator between both which gives rise to about 33 dB of gain. It also includes a microstrip bandpass filter. Figure 15 shows the characteristics of the gain module. It can be seen that the module has a gain of about 33dB across the entire band. The input return loss is better than -10dB and the output return loss is better than -7dB.

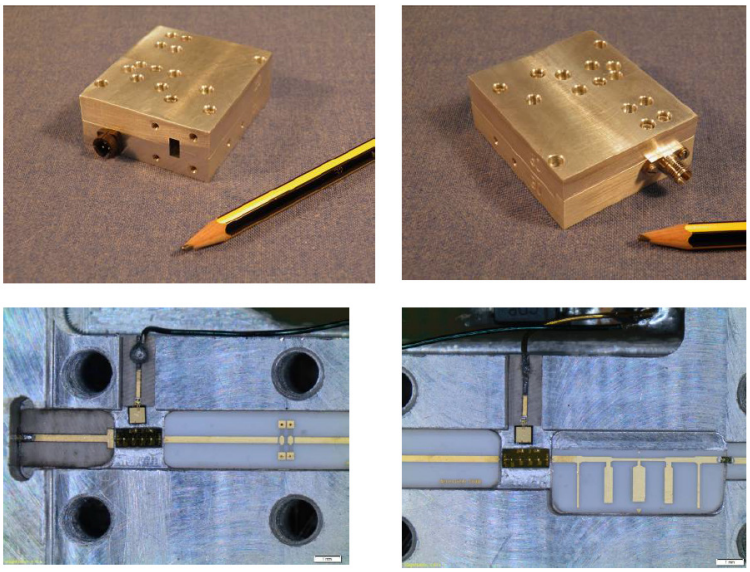

Figure 14. Photos to show the housing (top), MMIC (bottom left) and filter (bottom right) used in the RF gain module.

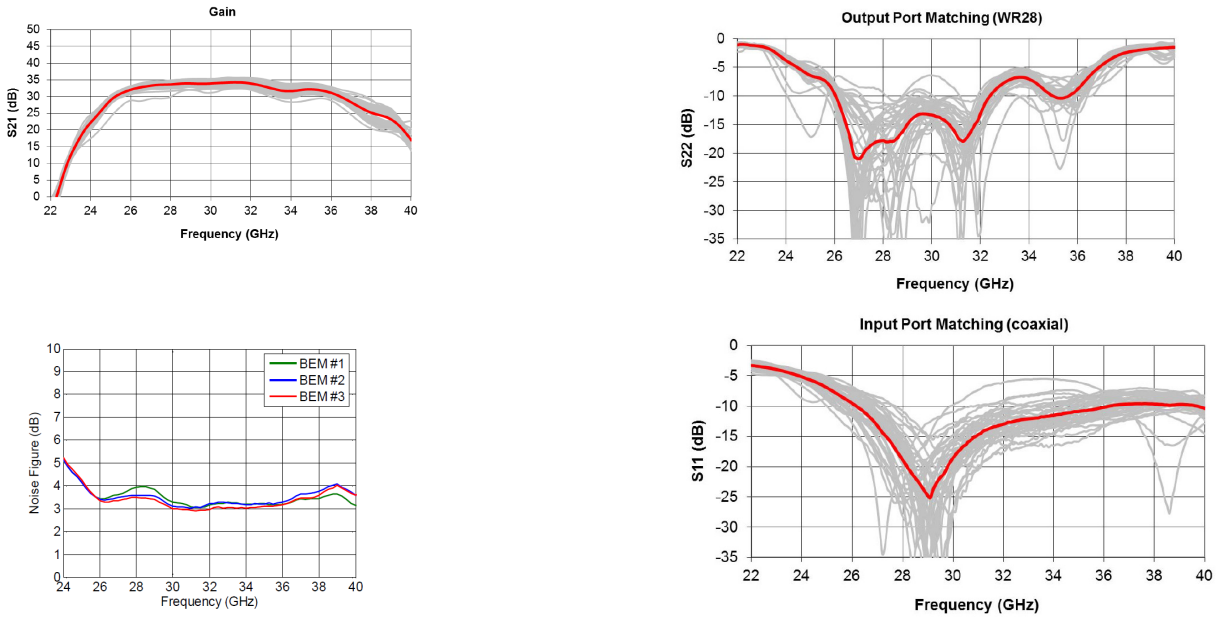

Figure 15. Graphs to show the s parameters of the RF gain module. Graphs show: (top left) Gain, (top right) output return loss, (bottom right) input return loss, (bottom left) noise figure.

4.6 Phase Switch Module

The phase switch module is made up of two 180º phase switches and two 90º phase switches. Figure 16 shows a photo of each of the 180º and 90º phase switches. It can be seen in the 3D drawing in figure 17 that the phase switches are placed in series with a waveguide input and output. Figure 18 shows the measured s parameters of the phase switch unit. It can be seen that the output return loss is better than -10dB across the whole band. The insertion loss is about -8dB. The top left graph shows the relative phase shift from a given phase state to 3 other phase states.

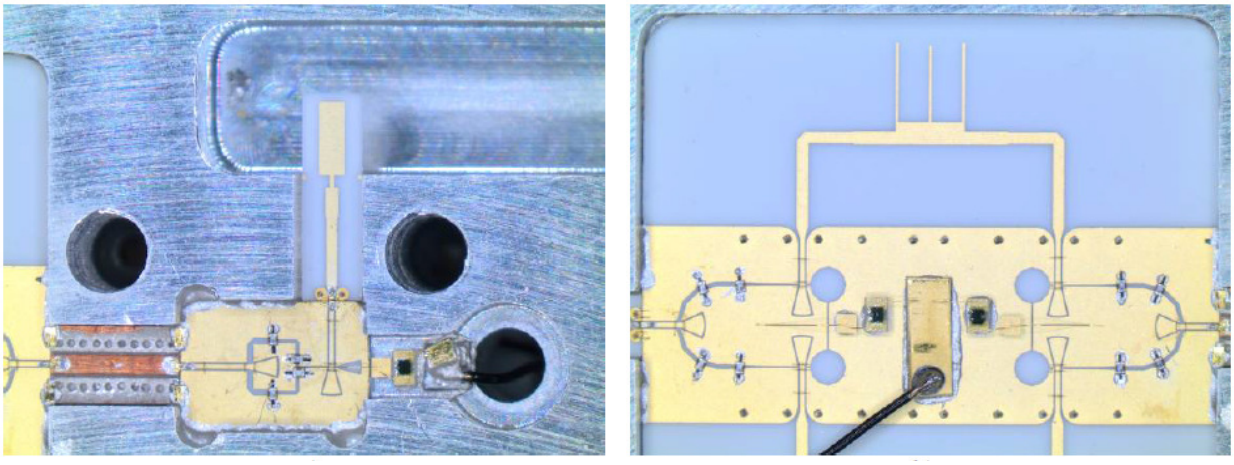

Figure16. Photos of the 180º (left) and 90º (right) phase switches

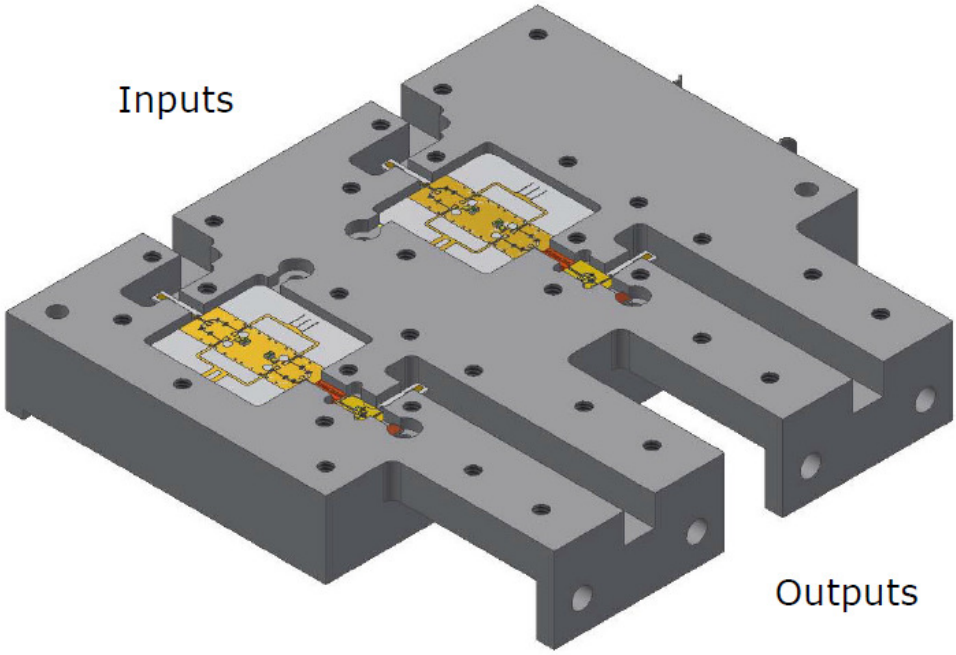

Figure 17. A 3D drawing of the phase switch housing showing the waveguide inputs and outputs

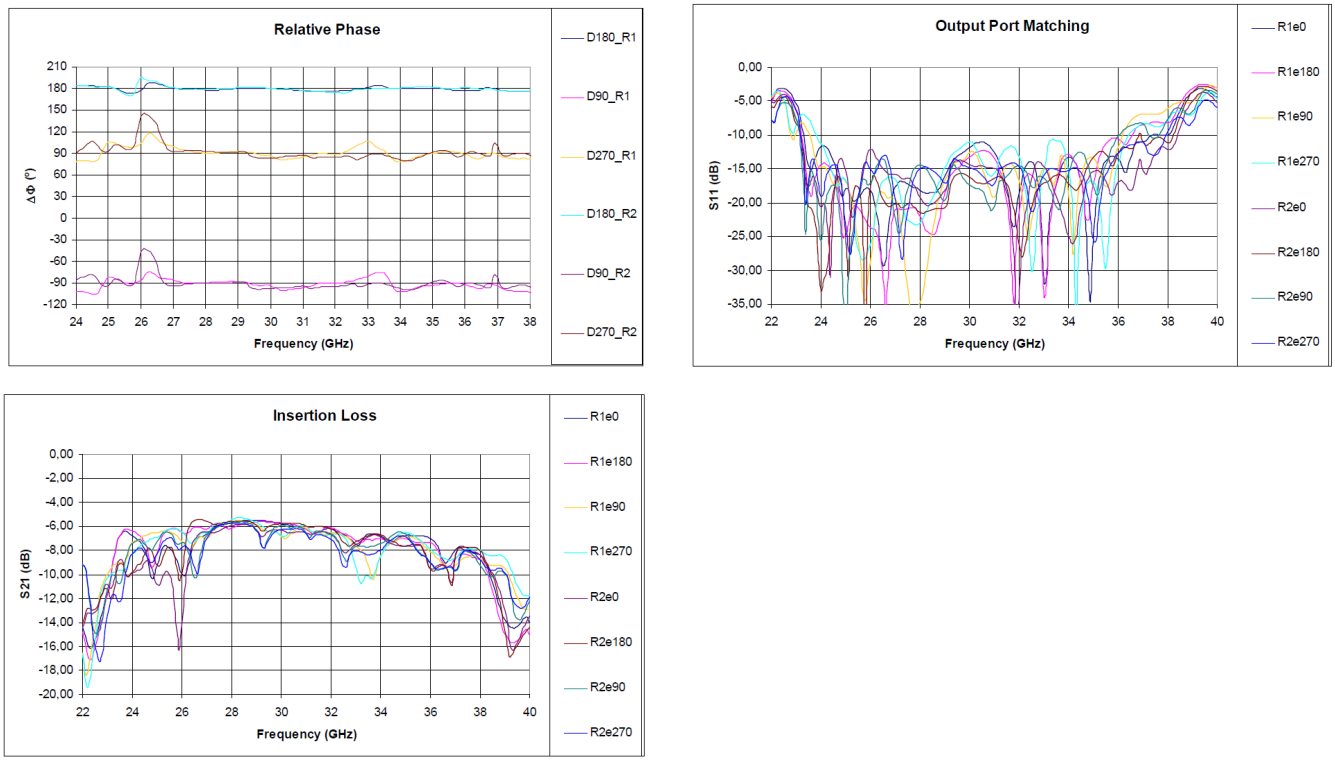

Figure 18. Graphs to show the s parameters of the phase switch unit. (Top left) Relative phase between phase states. (Top right) Output return loss. (Bottom left) Insertion Loss.

4.7 Detection Module

The detection module houses the complex correlator. Figure 19 (top left) is a photo of the complete unit and (top right) shows a close-up view of the microstrip hybrid coupler (ref). The module was tested with an equal amplitude and phase signal into the 2 input ports (Ex=Ey). Figure 19 (bottom left) shows a graph of the voltage output for a swept input signal. The 4 outputs are shown. It can be seen that there is cancelation in the X-Y channel and addition in the X+Y channel. The two remaining outputs give approximately half the signal of the X+Y output. The graph (bottom right) in figure 19 shows the linearity of the 4 output channels over the -26dBm to -10dBm generator input range (which is divided between the BEM inputs).

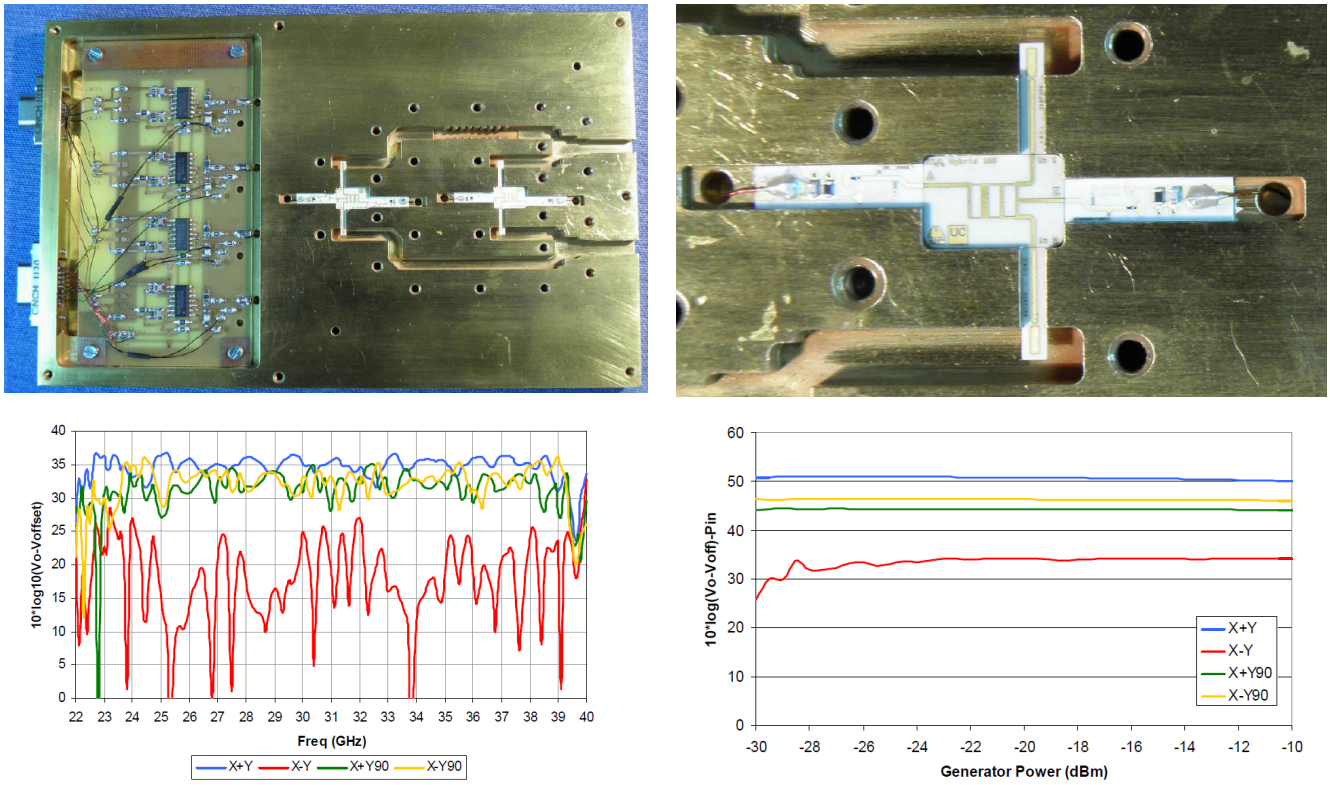

Figure 19. (top left) photo of the detection module without its top. (top right) Photo of the hybrid coupler in the detection module. (bottom left) Graph to show the 4 output voltages for a given frequency swept excitation (where Ex=Ey). (bottom right) Graph to show the linearity of the detector module.

4.8 BEM Rack

The BEM 19 inch rack houses the phase switches, the RF gain module and the detection module. Figure 20 shows a 3D drawing of (left) a single TGI BEM unit and (right) a set of 16 units housed in a 19 inch rack.

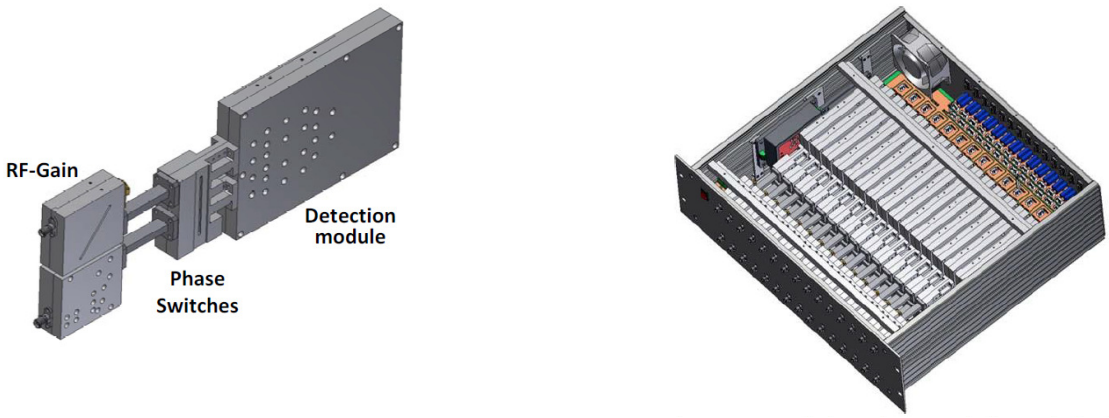

Figure 20. 3D drawings to show; (left) A single TGI BEM unit. (Right) 16 TGI BEMs housed in a 19 inch rack

One of the tasks that must be completed before designing and assembling a complete TGI pixel is to construct a power budget graph. Figure 21 shows the power budget for a TGI pixel. The power at the input is used as a starting point and the power at each stage along the chain is then calculated. Finally the signal arrives at the detector which has a window over which it has been shown to be linear. The power must be adjusted to fit within this window with margin for various observing situations.

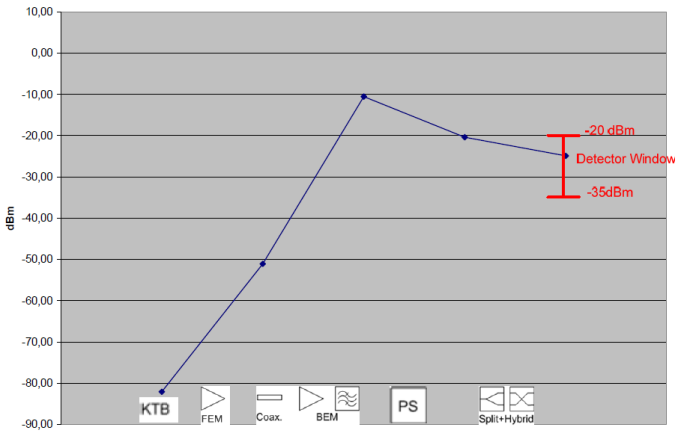

Figure 21. A graph to show the power budget for a TGI pixel taking the sky as an input reference.

5. PRE-COMISSIONING MEASUREMENTS AND REMAINING WORK

The TGI will be mounted on the telescope during summer 2014. It is currently in an advanced stage of manufacture. The most important tasks left are the manufacture of remaining cryogenic mechanical pieces and complete pixel integration and testing. A smaller test cryostat has already been assembled and tested. It is capable of holding 3 pixels at a time and will be used for cryogenic functionality test for complete pixels. Following tests on a subgroup of the 31 TGI pixels (eg 10 pixels) these pixels will be transferred to the TGI cryostat for final integration and calibration. Since the TGI design is completely modular, further subgroups can be added as and when the pixels are ready. The verification and calibration will first take place in the TGI cryostat at the IAC headquarters. Since it is difficult to provide a sky-equivalent load the background target will be at 300K. A calibration test bench has already been setup and proven to show a method for calibrating the TGI. There are 3 measurements that are particularly important to calibrate: the band shape, the polar isolation and polar angle, the linearity and T - Q/U leakage. Figure 22 shows a photo of the calibration test bench setup. A CW signal of known power is injected into one linear polarization of a feedhorn. The feedhorn is identical to the TGI feedhorn which is placed just in front of the other horn. Figure 23 shows the insertion loss and isolation of such a system. It can be seen that the bandpass is flat and the leakage into the orthogonal polarization is low < -40dB even when the horns are separated and offset by <1mm. This test was carried out in order to represent the situation in the cryostat where the TGI feedhorn cannot be seen and is also set back from the cryostat window. The photo also shows how different dielectric materials were placed in between the horns to see if there was any unforeseen effect. The graph in figure 22 shows that the properties hold well for this separation and misalignment.
With a flat swept source of a known power it is possible to measure the bandpass. The turntable encoder gives precise polar angle of the source which can be used to calibrate the TGI pixel. Using various levels of power input the linearity can be measured.

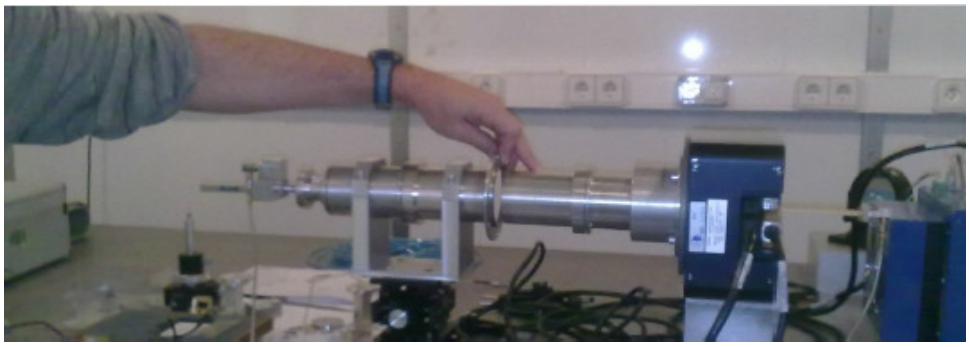

Figure 21. A photo of the TGI Calibration test bench showing the two feedhorns back to back. The right hand horn is placed inside a turntable so that the polar angle can be changed precisely. The left hand horn is mounted on a 3 axis XYZ positioner so that separation and offset can be simulated.

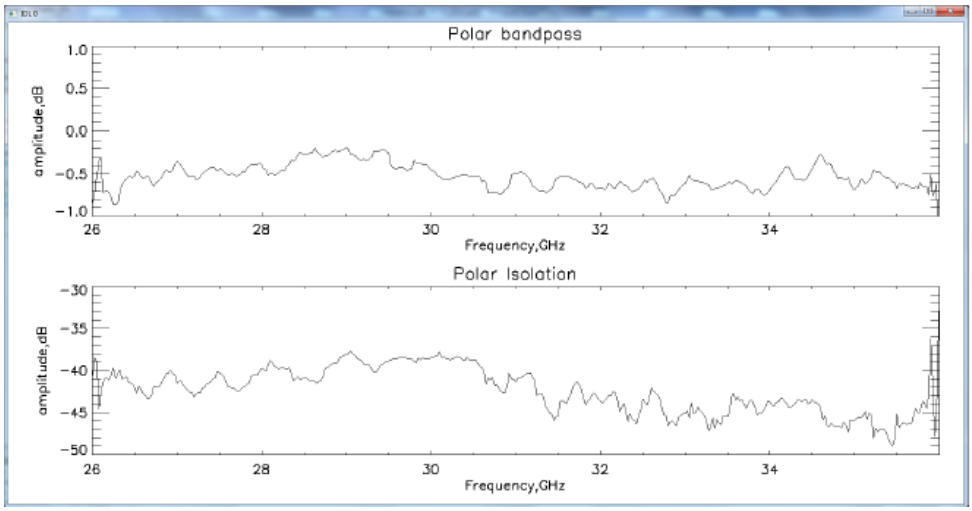

Figure 22. Graphs to show the insertion loss (top) and isolation (bottom) of the back to back feedhorn set up.

The calibration system will be used to calibrate the TGI when it has been cooled in the TGI cryostat at the IAC headquarters. Further verification will take place on the telescope on several pixels to show that nothing has changed in the transportation. The TGI will then be commissioned using astronomical sources. This work will take place by the end of 2014.

ACKNOWLEDGEMENTS

Special thanks to the IAC Mechanical workshop, for their help and contributions.

REFERENCES

[1] Tauber, J. A., Mandolesi, N., Puget, J. L., et al. " THE PLANCK MISSION," A&A, 520, A1 (2010)

[2] Kovac, J. M., Leitch, E. M., Pryke, C., Carlstrom, J. E., Halverson, N. W., and Holzapfel, W. L., "Detection of polarization in the cosmic microwave background using DASI," Nature 420, 772–787 (Dec. 2002).
[3] Rubiño-Martin, J.A. et al., "The QUIJOTE-CMB Experiment: studying the polarization of the Galactic and Cosmological microwave emissions," Society of Photo-Optical Instrumentation Engineers (SPIE) Conference Series (2012).
[4] Gomez-Renasco, F. et al., "Control system architecture of QUIJOTE multi-frequency instrument," Society of Photo-Optical Instrumentation Engineers (SPIE) Conference Series (2012).
[5] J. L. Cano, A. Tribak, R. Hoyland, A. Mediavilla, and E. Artal, "Full Band Waveguide Turnstile Junction Orthomode Transducer with Phase Matched Outputs", Int. Jrnl. RF and Microwave CAE, vol. 20, no. 3, May 2010, pp. 333-341.
[6] O´Dea et al., "Systematic errors in cosmic microwave background polarization measurements," MNRAS, 000, 1-19 (2007)
[7] B. Aja, et alt, "4-12 and 25-34-GHz Cryogenic mHEMT MMIC Low-Noise Amplifiers", IEEE Trans. on MTT, Vol 60, NO. 12, pp 4080-4088, Dec.2012.